A Modified Rough Interface Model Considering Shear and Normal Elastic Deformation Couplings

Article *in* International Journal of Solids and Structures · August 2020

DOI: 10.1016/j.ijsolstr.2020.07.013

2 authors, including:

Hamid Ahmadian
Iran University of Science and Technology
86 PUBLICATIONS **1,571** CITATIONS

SEE PROFILE

Dear Author

Please use this PDF proof to check the layout of your article. If you would like any changes to be made to the layout, you can leave instructions in the online proofing interface. Making your changes directly in the online proofing interface is the quickest, easiest way to correct and submit your proof. Please note that changes made to the article in the online proofing interface will be added to the article before publication, but are not reflected in this PDF proof.

If you would prefer to submit your corrections by annotating the PDF proof, please download and submit an annotatable PDF proof by clicking here and you'll be redirected to our PDF Proofing system.

International Journal of Solids and Structures xxx (xxxx) xxx

Contents lists available at ScienceDirect

International Journal of Solids and Structures

journal homepage: www.elsevier.com/locate/ijsolstr

A modified rough interface model considering shear and normal elastic deformation couplings

Hossein Jamshidi, Hamid Ahmadian *

Center of Excellence in Experimental Solid Mechanics and Dynamics, School of Mechanical Engineering, Iran University of Science and Technology, Narmak, Tehran 16848, Iran

ARTICLE INFO

Article history:
Received 28 January 2020
Received in revised form 24 June 2020
Accepted 20 July 2020
Available online xxxx

Keywords:
Flat rough surface
Elastic spherical asperities
Oblique contact
Hysteresis loop

ABSTRACT

This paper presents an analytical description of frictional contact hysteresis behavior between two flat rough surfaces in partial and gross slip. Couplings between shear and normal forces in the contact interface are included by considering spherical asperities in oblique contact. In the oblique contact, the relation between shear and normal interface forces is determined using asperities tangential friction forces and Hertzian normal contact forces. The Mindlin elastic spherical contact solution is modified in this study using the rod contact model leading to higher maximum tangential friction force and pre-slip limit compared to the classical solution. Based on the proposed modified Mindlin spherical contact solution, this paper develops a modified two rough interface (MTRI) model using the multi-asperity contact theory. The MTRI model provides accurate estimates of the contact interface behavior in an explicit form by including the oblique contact effects and the rod solution.

In obtaining the hysteresis behavior of two flat rough interface contact, the contact regions associated with the pre-slip and sliding state at different tangential loading phases, i.e., virgin loading, unloading, and reloading, are determined. Then by the integration of pairs of asperities contact forces over the contacting regions at each state, restoring forces of contacting surfaces are obtained. The proposed MTRI model predictions are validated against experimental observations and found to be in good agreement.

1. Introduction

The surface of all metals on the microscopic scale is rugged where the roughness or asperities have different height, gradient, and peak radii. The asperities geometry and the normal pressure of the interfaces affect the contact behavior and its associated friction coefficient (Panagouli and Mastrodimou, 2017). The asperities are not rigid and may have elastic or plastic deformations due to the shear and normal interaction forces between the two contact surfaces.

In shear contact between the two flat rough surfaces, the deformation is divided into states of partial and gross slips. In the partial slip region, the contact interface of some asperities is in stiction, while the contact in other asperities is in slip state. On the other hand, in the gross slip between the two flat rough surfaces, all asperities are in a complete slip mode (slide state). At the asperity scale, the contact mode is also divided into pre-slip (stick) and sliding modes. In the pre-slip mode, parts or whole contact area between two asperities is in stick state, while in the sliding mode, the entire contact area of asperities slips (Björklund, 1997; Eriten et al., 2011; Jankowski et al., 2016).

The statistical summation method is commonly employed in the analytical analysis of contact surface behavior. An important advantage of adopting a statistical summation method is that it relates contact parameters to the standard roughness measurement parameters. The resultant physical-based models are attractive in investigating the dynamic behavior of mechanical joints (Truster et al., 2013). The hysteretic response of contacts may be determined by concepts other than asperity models (Aleshin et al., 2018; Delrue et al., 2018). The latter methods are not the focus of this study.

There are two common scenarios in employing the statistical method, i.e., single rough surface (SRS) and two rough surfaces (TRS) (Greenwood and Tripp, 1970). The primary assumption in the SRS concept is that contact of all asperities is summit to summit. Consequently, the contact interface is simulated by a smooth flat rigid surface in contact with an elastic flat rough surface. These models do not consider the effects of asperities oblique contact and the two-contact topography coupling effects. Therefore phenomena such as coupling between vertical and horizontal contact

* Corresponding author.
E-mail address: ahmadian@iust.ac.ir (H. Ahmadian).

https://doi.org/10.1016/j.ijsolstr.2020.07.013
0020-7683/ 2020 Published by Elsevier Ltd.

Nomenclature

$\underline{R}$	the average radius of asperity summits
$\bar{R}$	the combined radius of asperity summits
σ	the standard deviation of asperity heights
$z, \bar{z}_{\max}$	asperity height and its maximum value
$\bar{z}_c$	the lowest height of contacting asperity
$\bar{z}_l$	slippage heights limit of asperity in the virgin loading phase
$\bar{z}_{l1}$	upper heights of sliding asperities in oscillating phase
$\bar{z}_{l2}$	the lower limit of asperity heights in stiction in the oscillating phase
r, r_o	the horizontal distance between axes of two contacted asperities and the initial value
y, y_o	distance between two flat rough surfaces and its initial value
ξ	overlap of two contacted asperities
θ	the contact angle of two contacted asperities
a	the radius of the contact area of two contacted asperities
$\bar{a}$	the normalized contact area of two contacted asperities
$\varphi, \bar{\varphi}$	the initial contact angle of two contacted asperities and its mean value
w	the penetration depth of two contacted asperities in the vertical direction
w_n	the penetration depth of two contacted asperities in the normal direction
η	the combined areal density of asperities
A	the nominal contact area of the rough interface
E, G	Young's modulus and shear moduli of contacting surface materials
$\bar{E}, \bar{G}$	combined Young's modulus and shear moduli
S, H	shear strength and hardness
ν	Poisson's ratios of contacting surface materials
R_a, R_q	mean and root mean square of roughnessSuperscripts M and B refer to Mindlin and Boltachev formulationsSubscripts u and l refer to the upper and lower contact surface
δ	the tangential relative displacement of two contacted asperities
δ_L	Slippage tangential displacement limit of two contacted asperities
v	the relative vertical displacement of two rough surfaces
u	the relative horizontal displacement of two rough surfaces
$\bar{u}$	the maximum relative horizontal displacement of two rough surfaces
u_L	slippage horizontal relative displacement limit of the flat rough interface
f_n	The Hertzian normal force of two contacted asperities
f_τ	tangential friction force of two contacted asperities
$f_{\tau,Max}$	slippage tangential frictional force limit of two contacted asperities
κ_1, κ_2	correction coefficient of slippage limits of displacement and friction force
p_a, q_a	vertical and horizontal force component of asperity
P_v, Q_v	the total vertical and horizontal force of rough interface in the virgin loading phase
P_o, Q_o	the total vertical and horizontal force of rough interface in the oscillatory loading phase
μ	friction coefficient
ψ	plasticity index
$\Phi(z)$	the probability density function of asperity heights
$\Psi(\varphi)$	the distribution function of the initial contact angle
γ	the ratio of combined radius to asperity radius
ε	variation of external vertical load
L_t, L_s	traversing and sampling length of the measured profile
R_{ku}	Kurtosis of the measured roughness profile
R_{Pc}	peak count of measured surface profile
R_{sm}	mean value of profile elements width
R_{sk}	the skewness of measured roughness profile

forces and the lift-up that are considered in this research cannot be modeled and investigated using the SRS strategy.

The TRS models consider both contact surfaces are rough and provide means to calculate contact normal and shear forces, as well as their associated normal and shear stiffness (Abdo, 2006). The main features of TRS models are that they simulate the oblique contact effect of asperities and consider the elastic interaction of two flat surfaces. The TRS model was first employed to describe the normal force between two contact surfaces (Greenwood and Tripp, 1970). In this modulation, Hertz forces were considered as the only interaction force between two asperities (Sepehri and Farhang, 2008; Sepehri and Farhang, 2011a). Elastic-plastic modeling of two flat surfaces using the finite element method was also carried out by these researchers (Sepehri and Farhang, 2011b). De Moerlooze et al. (2010) have introduced a model to simulate coupling between shear and normal directions of contact. They showed relative horizontal displacement in the contact interface of two rough surfaces creates movement in the vertical direction. This phenomenon was recorded in some experimental observations and is called "displacement lift-up" (Al-Bender et al., 2012). Ahmadian and Mohammadali (2016) have also conducted a set of studies on lift-up modeling. They provided a surface contact model that takes into account the coupling between shear and normal contact forces. Another study related to lift-up is the experimental research published by Hintikka et al. (2016). Gao et al. (2017) proposed the normal damping model of joint interfaces using the TRS model considering the pre-slip state and asperities in lateral contact. Empirical studies of Ahmadian and Mohammadali (2016), Al-Bender et al. (2012), and De Moerlooze et al. (2010) simulation show shear deformation affects the normal direction behavior in the pre-slip state of the contact interface. In addition, these studies indicate the TRS model simulates the lift-up phenomenon, while the SRS model ignores this phenomenon.

Many research works conducted on the TSR model neglect the pre-slip state in the investigation of frictional hysteresis behavior. However, there exist several methods to determine the tangential force of pre-slip in contact problems. Hills et al. (2018) proposed a family of techniques for the solution of a pure shear half-plane pre-slip problem. Mindlin et al. (1951) proposed a force–displacement relation in the pre-sliding state for the tangential force of virgin and oscillatory loading phases. Also, a tangential force–displacement relationship is proposed by Boltachev et al. (2012) based on the rod solution in the contact of two elastic spherical particles.

This paper provides a distributed model that considers the coupling effects between contact interface normal and friction forces and is capable of simulating the contact interface behavior, including hysteresis phenomena under constant and variable vertical loads. Instead of using classical Mindlin solution, a modified Mindlin solution is developed and employed to simulate the contact hysteresis behavior more accurately. The classical Mindlin solution of tangential friction force that is based on the Hertzian normal contact force theory is modified using the normal contact force

Please cite this article as: H. Jamshidi and H. Ahmadian, A modified rough interface model considering shear and normal elastic deformation couplings, International Journal of Solids and Structures, https://doi.org/10.1016/j.ijsolstr.2020.07.013

of the rod solution (Boltachev et al. 2012). Coupling effects due to the oblique contact of asperities are modeled by considering the asperities contact angle and the deformation friction coefficient in the contact interface formulation.

The asperity contact forces are evaluated for different states of the pre-slip and slip motion in three tangential loading phases, i.e., virgin loading, unloading, and reloading. Then the extracted relations are extended to surface contact interface using the integration of distribution function of asperity height. Finally, the results of this analytical model are verified by the experimental observations. Verifications are performed using two experimental studies where the first test case is a contact interface with constant vertical force. In this case, the hysteresis curves obtained from the proposed model are compared with the results of experimental data, where the parameters of the contact model are measured directly from contact interface topography, as reported by Eriten et al. (2011). The latter test case experiences variable vertical forces (Rajaei and Ahmadian, 2014), and it is shown the model presented in this paper is capable of simulating hysteresis behavior of the contact and its associate lift-up curves accurately.

The remaining of this paper is organized as follows: In Section 2, the geometrical and force relations in the contact interface of two spheres are reviewed. A new tangential friction force model is presented based on the classical Mindlin theory and the rod solution. Also, the oblique contact effect is modeled by considering the contact angle and the modified friction coefficient. In Section 3, contact forces of two flat rough surfaces are derived at asperities pre-slip and slip states. The predictions of the developed contact interface model of this study are validated in Section 4 using two experimental case studies. Finally, Section 5 draws some conclusions.

2. Contact of two spherical asperities

This section introduces the geometric properties of two contacted asperities and their associated normal and tangential contact forces. Fig. 2 shows the radius of the asperity summit and its height designated by R_u, R_l and z_u, z_l, respectively, subscripts u and l denote the upper and lower surfaces.

Fig. 2 shows the contact geometry of two asperities in two-dimensional coordinates. The distance between the mean asperity heights of contacting surfaces is y. Parameters θ and r, respectively, show the contact angle of the two spherical surfaces and asperities horizontal relative position; r_o shows the initial value of r. Assuming the overlap of two asperities is ξ, then:

$$\begin{aligned} &\xi = z - y, \\ &z = z_u + z_l, \\ &y = y_o + v. \end{aligned} \tag{1}$$

Parameter y_o shows the initial vertical distance between two flat surfaces and v is the relative vertical displacement of two rough surfaces. Using geometrical information of Fig. 1 and Fig. 2, the penetration depth is determined as,

$$w = \boldsymbol{Z}_l(r_l) + \boldsymbol{Z}_u(r_u) - y, \tag{2}$$

where,

$$\begin{aligned} &\boldsymbol{Z}_i(r) = z_i - R_i + \sqrt{R_i^2 - r^2},\ (i = l, u), \\ &r_l = \tfrac{R_l}{R_s} r,\ r_u = \tfrac{R_u}{R_s} r,\ R_s = R_l + R_u. \end{aligned} \tag{3}$$

The vertical penetration depth is calculated by substituting Eq. (1) and Eq. (3) into Eq. (2) as,

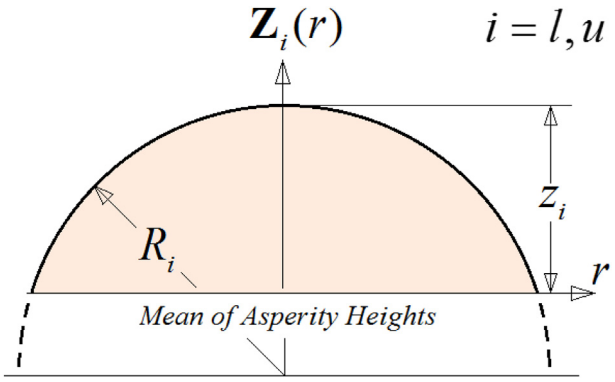

Fig. 1. Single spherical asperity geometry.

$$w \cong z - y - \frac{r^2}{2R_s}. \tag{4}$$

Eq. (4) enables one to define restoring forces of the considered contact interface.

2.1. Modified Mindlin tangential force

Classical Mindlin formulation defines the tangential friction force of two contacting spheres in pre-slip condition as (Johnson, 1987),

$$f_\tau^M = \mu f_n \left(1 - \left(1 - \frac{16\, a\, \bar{G}}{3\, \mu f_n}\delta\right)^{3/2}\right). \tag{5}$$

In Eq. (5), which states virgin loading friction force, superscript M represents Mindlin solution, μ, is the friction coefficient at the asperity scale, δ denotes the tangential displacement, and a is the radius of the contact area. Also the combined shear moduli, $\bar{G}$, is defined using shear moduli and Poisson's ratio of upper and lower contact surfaces, i.e., G_u, G_l, v_u, and v_l, as,

$$\bar{G} = \left((2 - v_l)G_l^{-1} + (1 - v_u)G_u^{-1}\right)^{-1}. \tag{6}$$

The Hertzian normal force, f_n, is defined as (Greenwood and Tripp, 1970),

$$f_n = K\, w_n^{3/2}, \quad K = \frac{4}{3}\bar{E}\sqrt{\bar{R}}, \tag{7}$$

where w_n is the normal penetration depth, and,

$$\bar{E} = \left((1 - v_l^2)E_l^{-1} + (1 - v_u^2)E_u^{-1}\right)^{-1},\ \bar{R} = \left(R_l^{-1} + R_u^{-1}\right)^{-1}. \tag{8}$$

In Eq. (5), the maximum tangential displacement and friction force in stick state are:

$$\delta_L^M = \frac{3\,\mu f_n}{16\, a\, \bar{G}}, \quad f_{\tau,Max}^M = \mu f_n. \tag{9}$$

Then Eq. (5) may be rewritten using the sign function of the horizontal contact relative velocity, $s = sign(\dot{u})$, in the following form:

$$f_\tau^M = s f_{\tau,Max}^M \left(1 - \left(1 - \frac{\delta}{\delta_L^M}\right)^{3/2}\right). \tag{10}$$

When two asperities are of similar material properties and identical summit radius, considering

$$E = 2\,G\,(1 + v),\ R_l = R_u = R, \tag{11}$$

Please cite this article as: H. Jamshidi and H. Ahmadian, A modified rough interface model considering shear and normal elastic deformation couplings, International Journal of Solids and Structures, https://doi.org/10.1016/j.ijsolstr.2020.07.013

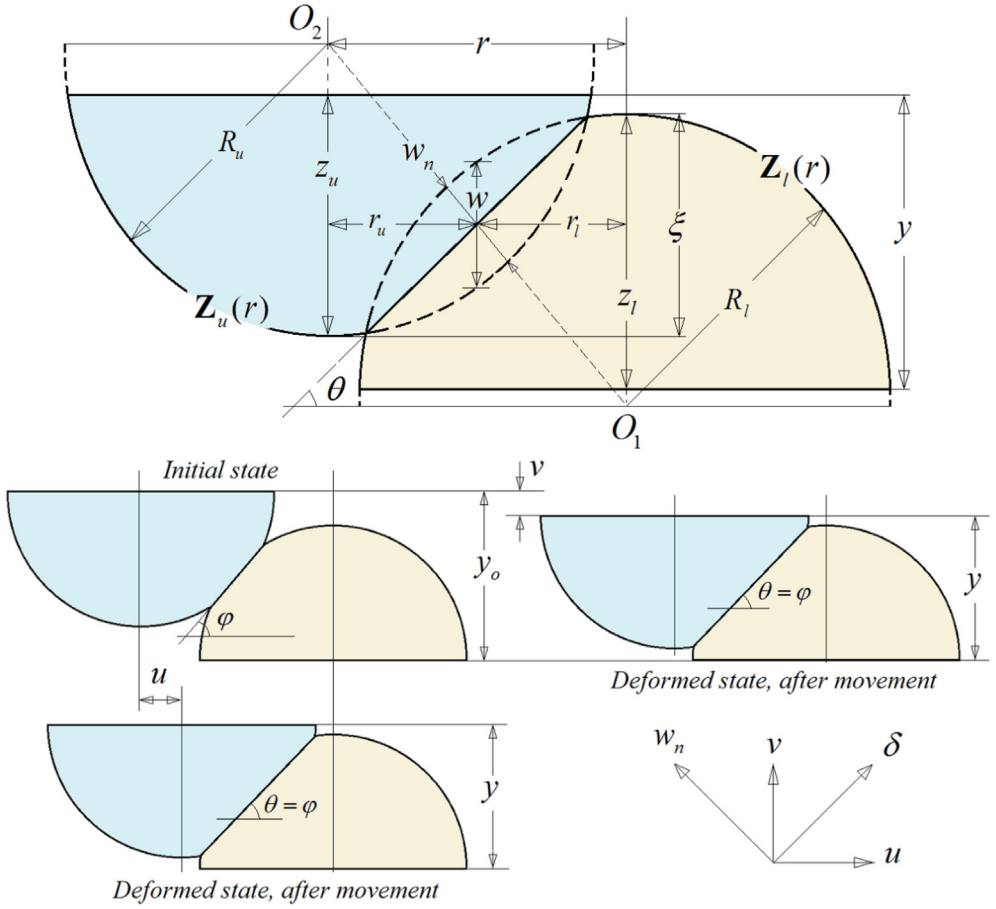

Fig. 2. Two asperities contact geometry.

then the maximum frictional force and the pre-slip tangential displacement limit based on the Mindlin theory is defined in the following forms:

$$\delta_L^M = \mu\frac{2-\nu}{1-\nu}\frac{a^2}{R},\ f_{\tau,Max}^M = \mu f_n = \frac{4}{3}\mu\frac{E}{1-\nu^2}\frac{a^3}{R}. \tag{12}$$

Compared to the classical Hertz law, a more recent model, i.e., the rod model (Boltachev and Aleshin, 2013), applies to a broader range of deformations. Based on the rod model, the deformation and stress distribution in the normal compression of spherical particles are sums of the Hertz solution, and the solution for the compression of a confined rod causes the relatively considerable deformations. Boltachev and Aleshin (2013), considered virtual rod reactions to the normal contact forces of elastic spherical particles in addition to the Hertz solution and proposed a new tangential force–displacement relation in the pre-slip state in an implicit form. Boltachev model predicts higher slippage friction force and displacement limit in the contact of two elastic spherical particles compared to the Mindlin solution. However, Boltachev model implicit formulation cannot be analytically integrated over asperity contacts of two rough interfaces using associated distribution functions. The present study reformulates the Mindlin explicit solution defined in Eq. (10) to overcome this difficulty by introducing correction factors to match Boltachev model maximum tangential friction force and pre-slip limit. This study shows the proposed modified Mindlin explicit formulation closely follows predictions of Boltachev implicit formulation and exactly matches its maximum tangential friction force and pre-slip limit. The modified Mindlin solution may be analytically integrated over asperity contacts of two rough interfaces using related distribution functions and predicts friction forces as accurate as Boltachev implicit formulation.

Boltachev et al. (2012) defined the maximum tangential friction force and pre-slip limit in the contact of two elastic spherical particles as:

$$\begin{aligned}\delta_L^B &= \mu\tfrac{2-\nu}{1-\nu}\tfrac{a^2}{R}\left(1+\tfrac{(1-\nu)^2}{1-2\nu}\tfrac{\operatorname{atanh}(2\bar{a})-2\bar{a}}{\bar{a}^2}\right),\quad \bar{a}=\tfrac{a}{2R},\\ f_{\tau,Max}^B &= \tfrac{4}{3}\mu\tfrac{E}{1-\nu^2}\tfrac{a^3}{R}\left(1-\tfrac{3\pi}{32}\tfrac{(1-\nu)^2}{1-2\nu}\tfrac{4\bar{a}^2+Ln(1-4\bar{a}^2)}{\bar{a}^3}\right),\end{aligned} \tag{13}$$

where superscript B refers to Boltachev formulation. Comparing Eq. (12) and Eq. (13), the present study relates the maximum tangential displacement of the two formulations using correction factors κ_1 and κ_2 as,

$$\delta_L^B = \kappa_1\delta_L^M,\qquad \kappa_1 = 1+\frac{(1-\nu)^2}{1-2\nu}\frac{\operatorname{atanh}\left(2\bar{a}\right)-2\bar{a}}{\bar{a}^2}, \tag{14}$$

and

$$f_{\tau,Max}^B = \kappa_2 f_{\tau,Max}^M,\quad \kappa_2 = 1-\frac{3\pi}{32}\frac{(1-\nu)^2}{1-2\nu}\frac{4\bar{a}^2+Ln\left(1-4\bar{a}^2\right)}{\bar{a}^3}. \tag{15}$$

Consequently, the tangential force–displacement relation based on rod model presented by Boltachev formulation is approximated by the modified Mindlin form,

Please cite this article as: H. Jamshidi and H. Ahmadian, A modified rough interface model considering shear and normal elastic deformation couplings, International Journal of Solids and Structures, https://doi.org/10.1016/j.ijsolstr.2020.07.013

$$f_\tau^B = s f_{\tau,Max}^B \left(1 - \left(1 - \frac{\delta}{\delta_L^B}\right)^{3/2}\right), \tag{16}$$

or:

$$f_\tau = s\,\kappa_2 f_{\tau,Max}^M \left(1 - \left(1 - \frac{\delta}{\kappa_1\,\delta_L^M}\right)^{3/2}\right). \tag{17}$$

Parameters κ_1 and κ_2, are correction coefficients which modify the classical Mindlin formulation, proposed in the present study. The slippage displacement limit δ_L^M defined in Eq. (12) for identical summit radius ($\bar{R} = R/2$) is,

$$\delta_L^M = \mu \frac{2-\nu}{2-2\nu} w_n. \tag{18}$$

In Fig. 3, the tangential friction force in contact of two spherical asperities determined using Eq. (17) is compared with Boltachev formulation and classical Mindlin solution in non-dimensional form. Parameters of the contact interface in this comparison are $\bar{a} = 0.2$ and $\nu = 0.25$. Fig. 3 shows the modified Mindlin explicit formulation closely follows the Boltachev implicit formulation predictions and exactly matches its maximum tangential friction force and pre-slip limit. At the same time, classical Mindlin solution underestimates the slippage limits of displacement and friction force. The proposed modified Mindlin solution of the present study may be analytically integrated over asperity contacts of two rough interfaces using related distribution functions and predicts friction forces as accurate as of the Boltachev implicit formulation.

The stick state force–displacement relation in of Eq. (17) is defined using the relative tangential displacement of asperities δ. It is noted that horizontal relative displacements of all asperities are identical and equal to the horizontal relative displacement of the rough upper surface u. When two asperities slip relative to each other, the contact angle between them varies. However, during the top surface movement, some contacting asperities are in gross slip state while others are in the pre-slip state. In the high amplitude of relative horizontal movement, the contact angles of all contacting asperities are varied. But in low movement amplitudes ($u \ll R$), when all the asperities are in the pre-slip state, the variation of contact angles are assumed to be negligible (as shown in Fig. 2, and they remain equal to the initial contact angle φ,

$$\varphi = \theta(r)|_{r=r_o}. \tag{19}$$

Therefore, the relative tangential displacement of two asperities in the stick state, expressed by δ, is obtained in terms of horizontal displacement u as,

$$u = \delta\,\mathrm{Cos}\varphi\,. \tag{20}$$

Substituting Eqs. (7), (18), (20) in Eq. (17) results:

$$f_\tau = s\,\mu\,\kappa_2 K w^{3/2} \mathrm{Cos}^{3/2}\varphi \left(1 - \left(1 - \frac{u}{\kappa_1 \lambda w\,\mathrm{Cos}^2\varphi}\right)^{3/2}\right). \tag{21}$$

Eq. (21) is the modified tangential friction force in the virgin loading phase, employed to predict the friction forces in saturated and unsaturated slip state (see Appendix A for more details).

In the following, variations of correction coefficient of slippage displacement and friction force, are investigated vs. normalized interference and contact area radius, in a wide range of Poisson ratios. As shown in Figs. 4 and 5, the correction factors κ_1 and κ_2, change smoothly and continuously vs. the asperity height deformation, and the contact area radius, in a wide range of Poisson's ratios. In Figs. 4 and 5, the asperity deformation is normalized by the asperity height standard deviation σ, and the contact area radius is normalized by the asperity radius. These two correction coefficients are always larger than unity ($\kappa_1 > 1,\ \kappa_2 > 1$) since the Mindlin model contact force predictions are lower than the Boltachev contact model estimates. These coefficients approach unity, i.e. $\kappa_1 \to 1,\ \kappa_2 \to 1$, as the normal contact force and resultant penetration depth decrease. The increase in the penetration depth of asperities causes the values of these coefficients to grow monolithically.

Due to the absence of singularities and abrupt changes in the correction factors, Eq. (21) may be employed for all domains of asperities heights in rough surfaces.

2.2. Friction coefficient model

The friction coefficient on the asperity scale μ, is used in Section 2.1 to define friction forces. This study employs a deformation dependent friction coefficient to determine friction forces. In general, the friction coefficient is composed of three components of adhesion μ_a, plowing μ_p, and asperity deformation μ_d. The plowing and deformation coefficients of frictions are due to the lateral contact of two asperities. The plowing part of the frictional force is a result of the penetration of hard asperities and is ignored in this study. Therefore, the total friction coefficient is assumed as:

$$\mu = \mu_a + \mu_d. \tag{22}$$

The adhesion friction coefficient is equal to the ratio of shear strength S to the hardness H of the softer material in the contact (Eriten et al., 2011),

$$\mu_a = \mathrm{S/H}. \tag{23}$$

The unites of both shear stress and hardness in Eq. (23) are Pascal (Pa). The deformation friction coefficient of two contacted spherical asperities is equal to (Halling, 1975):

$$\mu_d = 0.6\sqrt{\xi/R}. \tag{24}$$

The ratio of asperity overlap to its radius in the initial contact angle, shown in Fig. 2, is:

$$\xi/R = 2(1 - \mathrm{Cos}\varphi). \tag{25}$$

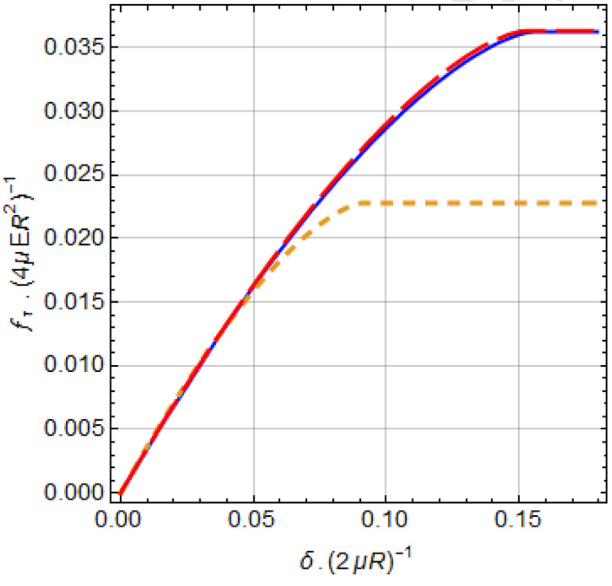

Fig. 3. Non-dimensional tangential force–displacement predictions; Modified Mindlin model (long-dashed line), Classical Mindlin solution (short-dashed line), Boltachev model prediction (solid line).

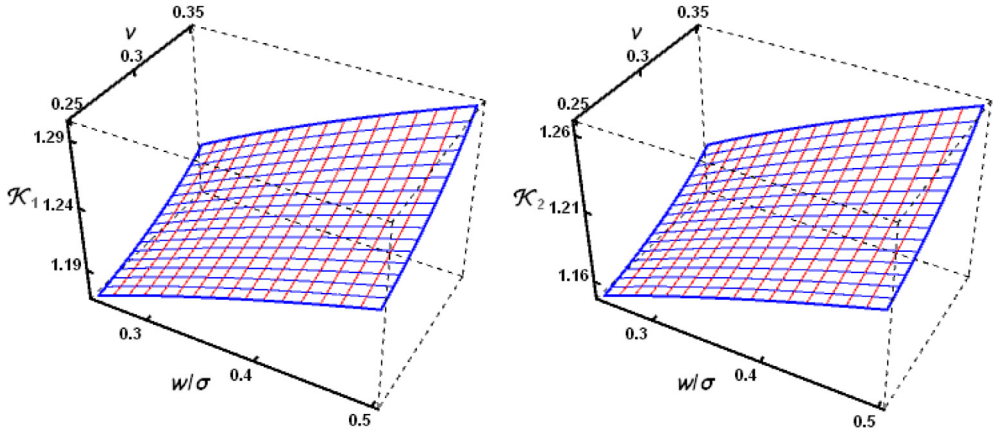

Fig. 4. The correction factors as functions of normalized asperity penetration depth and Poisson's ratio, a) displacement correction factor, b) friction force correction factor.

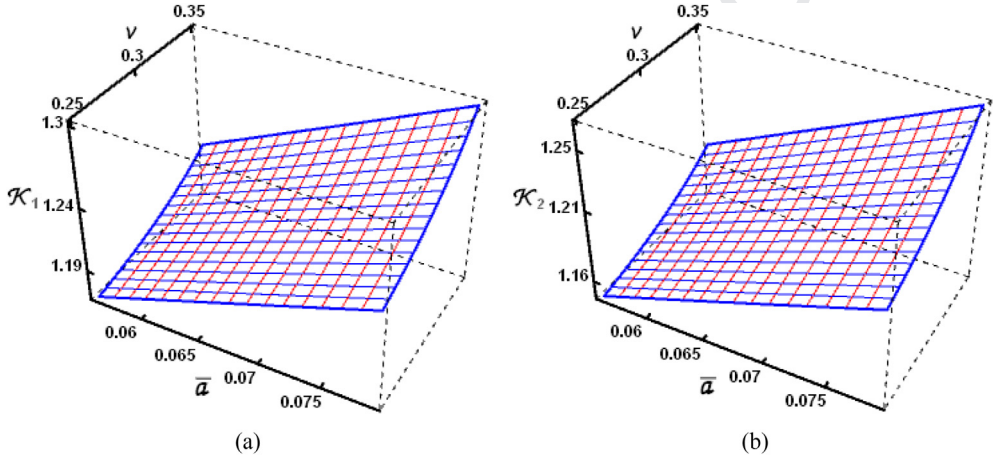

Fig. 5. The correction factors as functions of the normalized radius of the contact area and Poisson's ratio, a) displacement correction factor, b) friction force correction factor.

Consequently, the friction coefficient of Eq. (22) as a function of the contact angle is defined as:

$$\mu = \frac{S}{H} + 1.2\,\mathrm{Sin}\frac{\varphi}{2}. \tag{26}$$

The deformation friction coefficient due to lateral interaction of contacted spherical asperities is investigated numerically by Shi et al. (2016). The study shows the deformation friction coefficient varies proportionally to the contact angle variations. The deformation friction coefficient reaches to 0.15 at a contact angle of 20-degrees and by decreasing the contact angle to 15-degrees, μ_d approaches to 0.1. The modified tangential solution of Eq. (21) employs contact angle-dependent friction coefficient of Eq. (26) to predict the friction forces.

The SRI models assume the mean value of the initial contact angle φ in the contact of two rough surfaces, is small (Misra and Huang, 2012), and the slopes of surfaces are less than 10-degrees. The minimum value of the deformation friction coefficient, in this case, is assumed $\mu_d\left(\bar{\varphi} \simeq 10^\circ\right) = 1.2Sin(\pi/36) = 0.1$ (Hutchings and Shipway, 2017) and not equal to zero as deducted from Eq. (26). The resultant constant friction coefficient (CFC) model is:

$$\mu = S/H + 0.1. \tag{27}$$

It is noted that the asperity scale friction coefficient of Eq. (27) is always smaller than the macro slip friction coefficient of its corresponding rough interface. This is because the macro slip friction coefficient of a rough interface is obtained by considering the contacting surfaces are at the sliding state.

3. Contact forces of two flat rough surface

Eriten et al. (2011) used the classical Mindlin solution and developed a single rough surface (SRS) model based on the multi-asperity contact theory. This section adopts Eriten et al. (2011) strategy in establishing statistical contact force relations of asperities but considers the contact interface as two-rough surfaces (TRS) and uses the developed modified Mindlin contact force–displacement model. This study assumes the asperities are spherical, having the same radius and a known height distribution, as shown in Fig. 6. Underlying assumptions of the model are:

a) the deformation of the roughness remains in the elastic range, and Hertz theory is valid for the deformation ranges,
b) the geometry of asperities does not change due to their elastic deformations,
c) each asperity from a surface is contacted only with one asperity of the other surface, and
d) inertial effects of asperities are neglected.

Please cite this article as: H. Jamshidi and H. Ahmadian, A modified rough interface model considering shear and normal elastic deformation couplings, International Journal of Solids and Structures, https://doi.org/10.1016/j.ijsolstr.2020.07.013

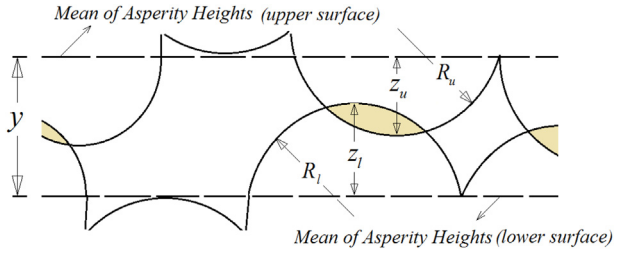

Fig. 6. Contact of two rough surfaces (asperities with different heights but similar radius).

The assumption of the rough elastic interface, assumption a), is based on actual behavior in structures; after initial plastic deformations, vibrations between contacting surfaces occur in an elastic state. Therefore, to achieve accurate simulations of frictional rough interface behavior in an oscillating motion, the rough surface parameters are measured after the interfaces being exposed to oscillatory loadings.

The height distributions of surfaces asperities are assumed to be Gaussian. Standard deviations of the asperity heights at upper and lower surfaces are denoted as σ_u and σ_l, respectively. The Gaussian probability density function of combined asperity heights, shown in Fig. 7, is:

$$\Phi(z) = \frac{1}{\sqrt{2\pi}\sigma} e^{-\frac{1}{2}\left(\frac{z}{\sigma}\right)^2}, \quad \sigma^2 = \sigma_u^2 + \sigma_l^2. \tag{28}$$

The following develops total vertical and horizontal forces in the contact of two flat rough surfaces. For this purpose, the asperities states of stick and slip at different contact interface region are obtained in two phases of virgin loading and oscillatory motion. Extracted relations between two asperities are extended to contact surface using the integration involving the Gaussian distribution function of asperity heights.

In the contact of two flat rough surfaces, some asperities are in contact and have positive penetration depth, i.e. $w > 0$, while the rest experience no contact. The minimum height for asperities in contact and with positive penetration depth, $\bar{z}_c$, is obtained using Eq. (4) as:

$$\bar{z}_c > y + \frac{r^2}{2R_s}. \tag{29}$$

Asperities with lower heights than $\bar{z}_c$ experience no contact with other asperities. The states of asperities in contact are different depending on their height and loading phase. In the virgin loading phase, as shown in Fig. 8, contacting asperities states are categorized as:

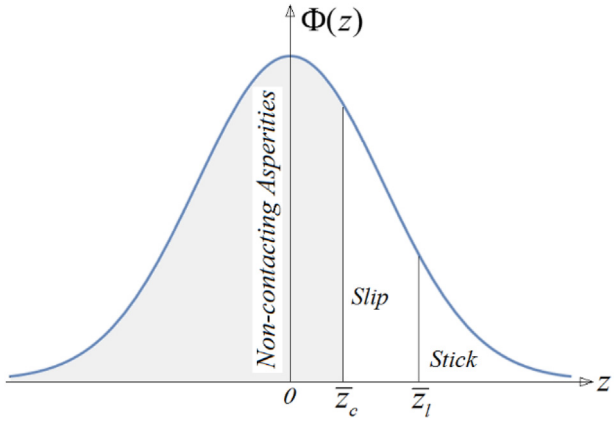

Fig. 8. Categories of asperities in virgin loading phase based on their heights distribution.

Category A: sliding asperities,
Category B: stick state asperities.

Fig. 8 shows the range of both categories A and B. The boundary between category A and B, displayed by $\bar{z}_l$, is determined by equating the stick and slip forces, $f_{\tau,l}^{stick} = f_{\tau}^{slip}$, defined in Eqs. (A.1) and (A.4) of Appendix A leading to:

$$\left(\kappa_1\left(\bar{z}_l\right)\lambda \mathrm{Cos}^2\varphi\right)\left(\bar{z}_l - y - \frac{1}{2R_s}(R_s\mathrm{Sin}\varphi - u)^2\right) = u. \tag{30}$$

The variation of displacement correction factor κ_1 as a function of asperity height is small and monotonic; therefore, by employing an average $\bar{\kappa}_1$ as:

$$\bar{\kappa}_1 = \frac{\int_{\bar{z}_c}^{\bar{z}_{\max}} \kappa_1 \Phi(z) dz}{\int_{\bar{z}_c}^{\bar{z}_{\max}} \Phi(z)\, dz}, \tag{31}$$

the boundary between stick and slip state is determined,

$$\bar{z}_l = y + \frac{1}{2R_s}\left(R_s\mathrm{Sin}\,\bar{\varphi} - u\right)^2 + \frac{u}{\bar{\kappa}_1 \lambda \mathrm{Cos}^2\,\bar{\varphi}}. \tag{32}$$

When $z > \bar{z}_l$ the two asperities are in stick, otherwise, they are in the slip state. Mean value of the initial contact angle of a rough interface φ is determined using the distribution of contact angles between the upper and lower asperities for isotropic interface (Misra, 2002),

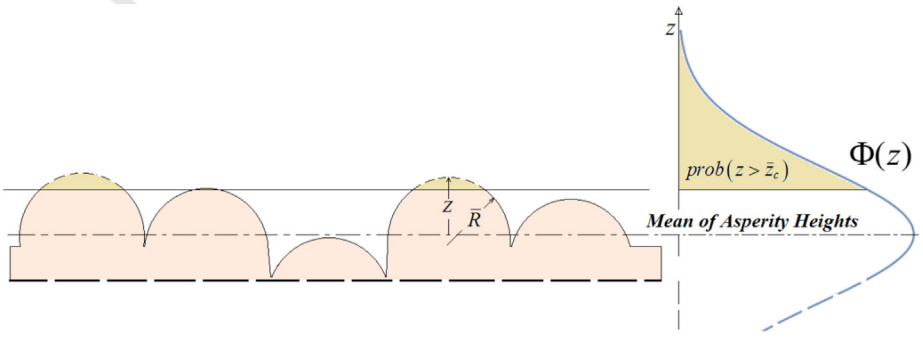

Fig. 7. Distribution of asperity heights of rough surfaces.

Please cite this article as: H. Jamshidi and H. Ahmadian, A modified rough interface model considering shear and normal elastic deformation couplings, International Journal of Solids and Structures, https://doi.org/10.1016/j.ijsolstr.2020.07.013

$$\Psi(\varphi) = \frac{\alpha\, Sin\alpha\,\varphi}{2\pi\, Sin\varphi}\left(1+\frac{\beta}{4}(3\,Cos2\alpha\,\varphi+1)\right), \quad 0 \leqslant \varphi \leqslant \frac{\pi}{2\alpha}, \quad \alpha \geqslant 1, \quad -1 \leqslant \beta \leqslant 2. \tag{33}$$

The parameters α and β are coefficients that describe, respectively, the extent and shape of the asperity contact orientations in the distribution function $\Psi(\varphi)$. A large value of α ($\alpha \to \infty$)represents a concentrated contact orientation, i.e., a zero mean value of contact angles,$\boldsymbol{E}[\varphi] = 0$, (Misra and Huang, 2011).

The maximum initial contact angle is generally within the range of $\pi/12 \leqslant \varphi < \pi/4$ (Misra and Huang, 2012), and its mean value, $\bar{\varphi}$, is defined as:

$$\bar{\varphi} = \int_0^{\frac{\pi}{2\alpha}} \varphi\, \Psi(\varphi)\, d\varphi, \quad \alpha \geqslant 2 \tag{34}$$

By substitution Eq. (33) in Eq. (34), it is shown that for $\alpha \geq 6$, the mean of contact angle equals,

$$\bar{\varphi} = \frac{6-\beta}{6\,\alpha}. \tag{35}$$

Fig. 9 shows vertical and horizontal forces, p_a and q_a, applied to the upper asperity and the vertical force ensures the non-separation of the asperity pairs. The vertical and horizontal forces in terms of tangential friction and Hertzian normal contact forces for all states of contact are:

$$\begin{cases} p_a = f_n\, Cos\theta + f_\tau\, Sin\theta \\ q_a = -f_n\, Sin\theta + f_\tau Cos\theta \end{cases}, \quad (r>0,\ \dot{r}>0). \tag{36}$$

The vertical and horizontal forces for each of the different contact states, i.e., pre-slip and slip states, as well as various loading phases, i.e., the virgin and the oscillatory loading phases, are provided in Appendix A. The horizontal and vertical forces due to the interaction between all asperities in the virgin loading phase are:

$$P_v(u,v) = \eta A \int_0^{\pi/2\alpha}\int_{z^-_c}^{z^-_l} p_a^{slip}(u,v,z,\theta)\,\Phi(z)\Psi(\varphi)dz\,d\varphi + \eta A \int_0^{\pi/2\alpha}\int_{z^-_l}^{z^-\max} p_{a,I}^{stick}(u,v,z,\varphi)\,\Phi(z)\Psi(\varphi)dz\,d\varphi, \tag{37}$$

and

$$Q_v(u,v) = \eta A \int_0^{\pi/2\alpha}\int_{z^-_c}^{z^-_l} q_a^{slip}(u,v,z,\theta)\,\Phi(z)\,\Psi(\varphi)\,dz\,d\varphi + \eta A \int_0^{\pi/2\alpha} \times \int_{z^-_l}^{z^-\max} q_{a,I}^{stick}(u,v,z,\varphi)\,\Phi(z)\,\Psi(\varphi)\,dz\,d\varphi. \tag{38}$$

Parameters A and η are nominal contact area and areal asperity density, respectively. It is noted in calculating the horizontal and vertical forces $\bar{z}_{\max} = 3\sigma$ is selected as it includes 99.73% of all asperities height.

Eqs. (37) and (38) establish the vertical and horizontal forces of the contact surface in virgin loading. Next, the contact forces in the oscillatory loading phase are considered where contacting asperities, as shown in Fig. 10, fall into one of three categories,

I. Asperities that slip at both unloading and reloading phases,
II. Asperities that are in stick state at unloading and slip at reloading, and also those that slip in unloading are in stick state at reloading,
III. Asperities that are always in stick state in the unloading and reloading.

As before, the boundary between asperity heights of category I and II is shown by $\bar{z}_{l1}$. The variable $\bar{z}_{l1}$ indicates the maximum height of asperities that are always in slip state and is called upper height in the slip region. The boundary between asperities of category II and III is shown by $\bar{z}_{l2}$. Similarly, the variable $\bar{z}_{l2}$ indicates the minimum height of asperities that are always in stick state and is called lower height in stick region. Quantities of $\bar{z}_{l1}$ and $\bar{z}_{l2}$ are obtained from the solution of force equilibrium equations. The lower stick boundary of asperity heights occurs when the amplitude of tangential force of the pre-slip state of unsaturated oscillatory loading phase (Eq. (A.3)) is equal to the tangential force of gross slip state (Eq. (A.4)), i.e.:

$$f_{\tau,III}^{stick}\Big|_{u=u^-} = f_\tau^{slip}. \tag{39}$$

This results in the lower stick boundary of asperity heights as:

$$\bar{z}_{l2} = y + \frac{1}{2R_s}\left(R_s Sin\,\bar{\varphi} - \bar{u}\right)^2 + \frac{\bar{u}}{\bar{\kappa}_1 \lambda\, Cos^2\,\bar{\varphi}}. \tag{40}$$

As shown in Fig. 10, for a situation where $z \geqslant \bar{z}_{l2}$ the contact of two asperities is always in stick state. In other words, contact of two spherical asperities is in category III.

Also, the upper slip boundary of asperity heights is obtained from the solution of the force equilibrium equation of Eqs. (A.2) and (A.4) as (Jankowski et al., 2016),

$$f_{\tau,II}^{stick} = f_\tau^{slip}. \tag{41}$$

Therefore the upper slip boundary is obtained as:

$$\bar{z}_{l1} = y + \frac{1}{2R_s}\left(R_s Sin\,\bar{\varphi} - u\right)^2 + \frac{\left(\bar{u}-u\right)}{2\bar{\kappa}_1 \lambda\, Cos^2\,\bar{\varphi}}. \tag{42}$$

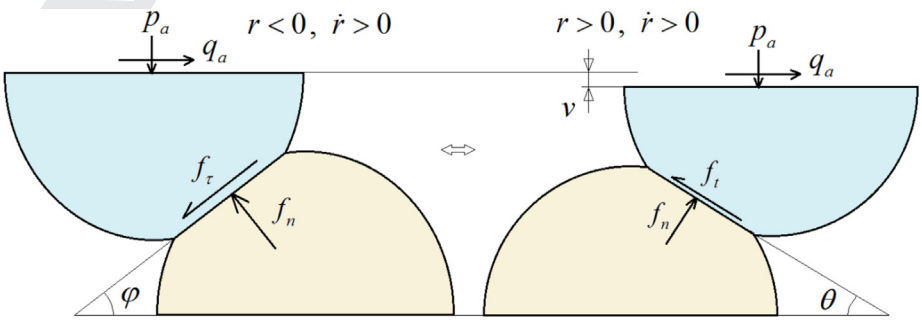

Fig. 9. Applied external forces on an asperity pair and the associated sliding motion.

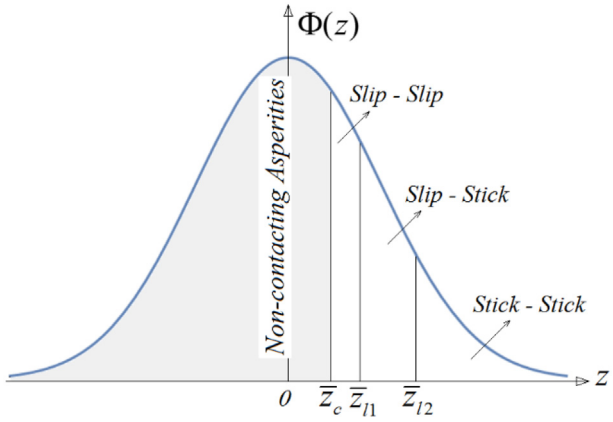

Fig. 10. Asperity heights distribution in unloading and reloading phase divided into three categories.

When $\bar{z}_c \leqslant z \leqslant \bar{z}_{l1}$, contact of two single asperities is always in slip situation, in other words, contact of two asperities falls into category I. Because κ_1 is a function of the asperity height, an accurate estimate of $\bar{z}_{l1}$ and $\bar{z}_{l2}$ is obtained when $\bar{\kappa}_1$ in Eq. (40) and Eq. (42) is replaced by $\kappa_1\left(\bar{z}_{l1}\right)$ or $\kappa_1\left(\bar{z}_{l2}\right)$ as,

$$\begin{aligned}\left(\kappa_1\left(\bar{z}_{l1}\right)\lambda\,\mathrm{Cos}^2\varphi\right)\left(\bar{z}_{l1}-y-\tfrac{1}{2R_s}\left(R_s\mathrm{Sin}\varphi-u\right)^2\right)&=\bar{u}-u,\\ \left(\kappa_1\left(\bar{z}_{l2}\right)\lambda\,\mathrm{Cos}^2\varphi\right)\left(\bar{z}_{l2}-y-\tfrac{1}{2R_s}\left(R_s\mathrm{Sin}\varphi-\bar{u}\right)^2\right)&=\bar{u}\,.\end{aligned}\tag{43}$$

The resultant horizontal and vertical forces due to the interaction of all asperities in oscillatory loading phase are:

$$\begin{aligned}P_o(u,v)=\eta A\int_0^{\pi/2\alpha}\int_{\bar{z}_c}^{\bar{z}_{l1}} p_a^{slip}(u,v,z,\theta)\,\Phi(z)\,\Psi(\varphi)\,dz\,d\varphi\\ +\eta A\int_0^{\pi/2\alpha}\int_{\bar{z}_{l1}}^{\bar{z}_{l2}} p_{a,II}^{stick}(u,v,z,\varphi)\,\Phi(z)\,\Psi(\varphi)\,dz\,d\varphi\\ +\eta A\int_0^{\pi/2\alpha}\int_{\bar{z}_{l2}}^{\bar{z}_{\max}} p_{a,III}^{stick}(u,v,z,\varphi)\,\Phi(z)\,\Psi(\varphi)\,dz\,d\varphi\,,\end{aligned}\tag{44}$$

and

$$\begin{aligned}Q_o(u,v)=\eta A\int_0^{\pi/2\alpha}\int_{\bar{z}_c}^{\bar{z}_{l1}} q_a^{slip}(u,v,z,\theta)\,\Phi(z)\,\Psi(\varphi)\,dz\,d\varphi\\ +\eta A\int_0^{\pi/2\alpha}\int_{\bar{z}_{l1}}^{\bar{z}_{l2}} q_{a,II}^{stick}(u,v,z,\varphi)\,\Phi(z)\,\Psi(\varphi)\,dz\,d\varphi\\ +\eta A\int_0^{\pi/2\alpha}\int_{\bar{z}_{l2}}^{\bar{z}_{\max}} q_{a,III}^{stick}(u,v,z,\varphi)\,\Phi(z)\,\Psi(\varphi)\,dz\,d\varphi\,.\end{aligned}\tag{45}$$

The proposed modified two rough interfaces (MTRI) model in Eqs. (37) and (38) and Eqs. (44) and (45) is valid for pre-slip and small gross slip region, i.e., for a low range of displacements, and also predicts the lift-up phenomenon.

The developed MTRI formulation is demonstrated and validated by performing numerical and experimental studies in the next section.

4. Simulation and verification

This section employs the proposed model to simulate contact forces and displacements of two flat rough surfaces under both constant and variable vertical loads. First, a numerical case study is presented to demonstrate the model capabilities in accounting for coupling between horizontal and vertical loads in the contact and its resultant lift up effects. The proposed model predictions are also validated against two different experimental observations. In the first experimental verification, the contact interface experiences a constant vertical force, while in the second set of experiments, the vertical contact force varies.

4.1. Numerical case study

The followings study demonstrate simulation results of the contact forces between two flat rough surfaces shown in Fig. 6 in two different modes of constant and variable vertical preload. Two flat rough surfaces are made of aluminum alloy with the material properties and surface characteristics specified in Table 1. It should be noted that in the contact of two rough surfaces, the combined rough surface parameters (σ, $\bar{R}$ and η) are calculated by asperity heights profiles (Eriten et al., 2011). The combined radius curvature may be larger than $\bar{R}$ defined by Eq. (8). Therefore by considering this fact in the contact interface profiles, the parameter γ is defined as,

$$\gamma=\frac{\bar{R}}{R}\geqslant\frac{1}{2}\,.\tag{46}$$

The horizontal displacement excitation of the top surface, u, and its vertical preload $\bar{P}$ are:

$$\begin{aligned}u&=\bar{u}\,\sin\omega t,\\ \bar{P}&=P_0(1+\varepsilon\sin\omega t).\end{aligned}\tag{47}$$

The harmonic motion u applied on the upper flat surface and resultant hysteresis curves are shown in Figs. 11 and 12, respectively.

The resultant hysteresis curves in Fig. 12 (a) in the presence of constant applied force, show that the overall behavior of obtained curves is in agreement with expected behavior dissipated energy of frictional interfaces. By increasing the amplitude of relative horizontal motions $\bar{u}$ while keeping the vertical force constant, the frictional curves changed from the unsaturated state (stick) into a saturated state (slip) at the amplitude of $\bar{u}=2.5\,\mu m$.

As seen in Fig. 12 (a), the friction limit of the proposed model is inclined downward very slightly in a constant normal force condition at $\bar{u}=2.5\mu m$. This small reduction of slippage friction limit is due to decreases of asperities contact angles during slip state; the horizontal component of asperities restoring forces decreases, and subsequently, the total friction force is decreased. This phenomenon happens when the slippage displacement limit of rough interface takes place at low horizontal amplitudes ($u \ll R$), and it is predicted by the MTRS model, in the reduction of contacts of the rough interface.

Fig. 12(b) shows the hysteresis curves under the variable vertical load. In the virgin loading phase and at the end of the reloading phase, when the normal force decreases, the distance of two contacting surfaces increase, and the number of contacting asperities decrease consequently. The reduction of the number of contacting asperities leads to a reduction of horizontal friction force.

Table 1
Material properties and topography parameters of contacting interface.

Surface roughness parameters		Material and structure properties ($i=u,l$)	
Value	Parameter	Value	Parameter
$5\mu m$	σ_i	$70\,Gpa$	E_i
$75\mu m,\ 0.5$	$R_i,\ \gamma$	0.3	v_i
$100\,mm^{-2}$	η	$10cm^2$	A
$10,\ 1$	$\alpha,\ \beta$	0.3	S/H

Please cite this article as: H. Jamshidi and H. Ahmadian, A modified rough interface model considering shear and normal elastic deformation couplings, International Journal of Solids and Structures, https://doi.org/10.1016/j.ijsolstr.2020.07.013

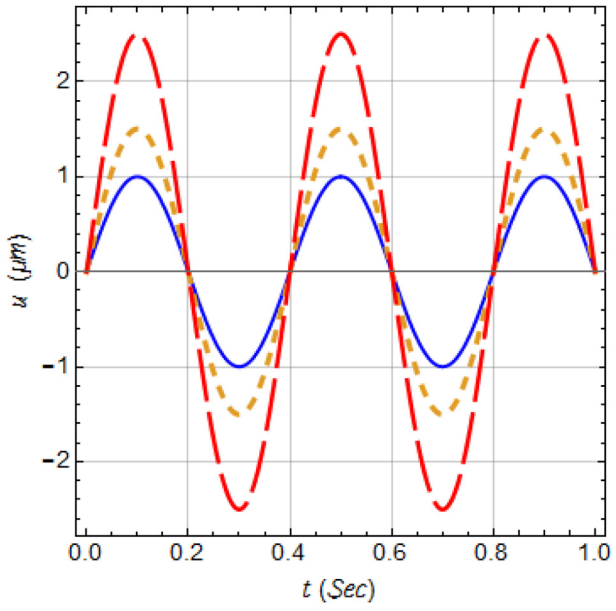

Fig. 11. Harmonic motion u applied on the upper flat surface ($\omega = 2.5\,Hz$) $\bar{u} = 1.0\mu m$(solid line), $\bar{u} = 1.5\mu m$(short-dashed line), $\bar{u} = 2.5\,\mu m$(long-dashed line).

The presented model also can simulate lift-up curves. The results of experimental studies have shown that in the pre-slip regime of two contact surfaces, the lift-up butterfly curves are produced (Al-Bender et al., 2012; Hintikka et al., 2016). The plots of vertical displacement vs. the horizontal movement and the horizontal force demonstrate the butterfly curves (Al-Bender et al., 2012). Lift-up butterfly curves for the interface specified in Table 1, are shown in Figs. 13 and 14 in constant and variable vertical force condition, respectively. This is the first analytical model that simulates the displacement lift-up and friction lift-up phenomenon. It should be noted that in a high variation of vertical force or cases where interface separation occurs, the lift-up event is not visible clearly, as their order of deformation magnitude is minimal compared to the deformations under vertical loading.

When the modeling of the butterfly lift-up phenomenon is not of prime interest, and the purpose of modeling is to extract friction hysteresis curves, the MTRI model may be simplified. At this case, the contact of asperities may be considered summit-to-summit, by assigning,

$$\varphi \simeq 0, \quad \theta = 0, \quad r_o = 0. \tag{48}$$

Because the SRS model ignores the effect of oblique contact of asperities, the accuracy of hysteresis friction force decreases. The contribution of the deformation friction coefficient (μ_d) must be included in the SRS model to prevent this deficiency. Thus, based on the proposed MTRI model, a modified SRS model is presented that is called modified single rough interfaces (MSRI) model. In the MSRI model, it is assumed the mean value of the initial contact angle φ in the contact of two rough surfaces, is small (Misra and Huang, 2012), and the slopes of surfaces are less than 10-degrees. Therefore the deformation friction coefficient is about 0.1 (Hutchings and Shipway, 2017), i.e.$\mu_d\left(\bar{\varphi} \simeq 10^{\circ}\right) = 1.2Sin(\pi/36) = 0.1$, and the resultant constant friction coefficient (CFC) of Eq. (27) is applied in the MSRI model.

The relation of friction forces of contacted asperities in the MSRI model are:

$$\begin{aligned}
q_I^{stick}(u,z) &= s\mu\kappa_2 K w^{3/2}\left(1-\left(1-\tfrac{1}{\bar{\kappa}_w}\tfrac{u}{w}\right)^{3/2}\right),\\
q_{II}^{stick}(u,z) &= -s\mu\kappa_2 K w^{3/2}\left(2\left(1-\tfrac{1}{2\bar{\kappa}_w}\tfrac{(su+\bar{u})}{w}\right)^{3/2}-1\right),\\
q_{III}^{stick}(u,z) &= -s\mu\kappa_2 K w^{3/2}\left(2\left(1-\tfrac{1}{2\bar{\kappa}_w}\tfrac{(su+\bar{u})}{w}\right)^{3/2}-\left(1-\tfrac{1}{\bar{\kappa}_w}\tfrac{u}{w}\right)^{3/2}-1\right),\\
q^{slip}(u,z) &= s\mu\kappa_2 K w^{3/2},
\end{aligned} \tag{49}$$

and total vertical and horizontal forces in the virgin and oscillatory loading phases in MSRI model are:

$$\begin{aligned}
P(v) &= K\eta A\int_{\bar{z}_c}^{\bar{z}_{\max}} w^{3/2}\,\Phi(z)\,dz.\\
Q_v(u) &= \eta A\left(\int_{\bar{z}_c}^{\bar{z}_l} q^{slip}(u,z)\,\Phi(z)\,dz+\int_{\bar{z}_l}^{\bar{z}_{\max}} q_I^{stick}(u,z)\,\Phi(z)\,dz\right).\\
Q_o(u) &= \eta A\left(\int_{\bar{z}_c}^{\bar{z}_{l1}} q^{slip}(u,z)\,\Phi(z)\,dz+\int_{\bar{z}_{l1}}^{\bar{z}_{l2}} q_{II}^{stick}(u,z)\,\Phi(z)\,dz\right.\\
&\left.+\int_{\bar{z}_{l2}}^{\bar{z}_{\max}} q_{III}^{stick}(u,z)\,\Phi(z)\,dz\right).
\end{aligned} \tag{50}$$

The boundary limits of asperities contact state are also equal to:

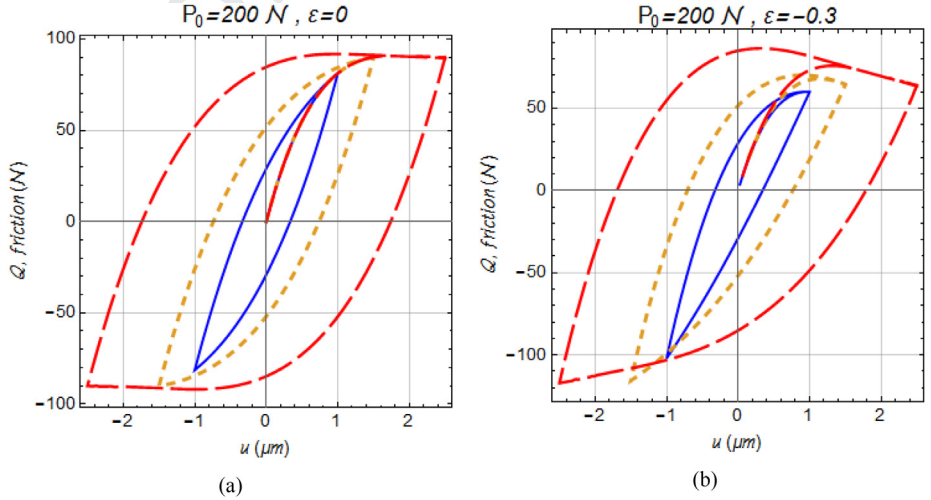

Fig. 12. Hysteresis curves at $\bar{u} = 1.0\mu m$ (solid line), $\bar{u} = 1.5\mu m$(short-dashed line), $\bar{u} = 2.5\,\mu m$(long-dashed line), a) constant vertical force, b) variable vertical force.

Please cite this article as: H. Jamshidi and H. Ahmadian, A modified rough interface model considering shear and normal elastic deformation couplings, International Journal of Solids and Structures, https://doi.org/10.1016/j.ijsolstr.2020.07.013

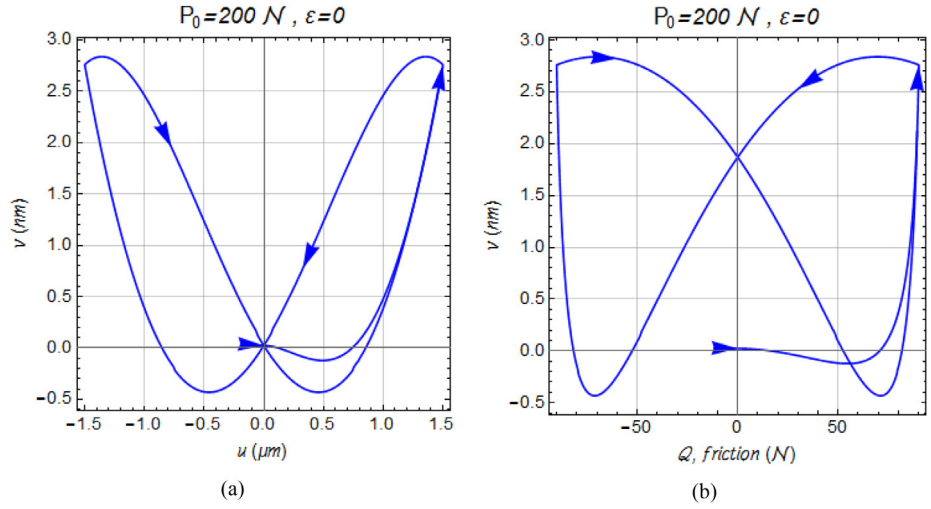

Fig. 13. Lift-up phenomenon predictions in constant vertical load, a) vertical displacement vs. horizontal displacement b) vertical displacement vs. horizontal friction force, (μ = 1.5 μm).

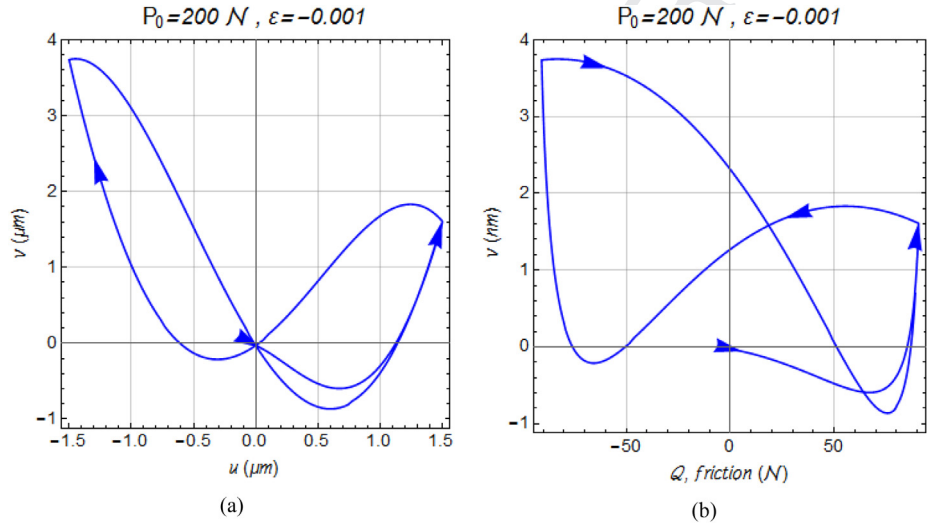

Fig. 14. Lift-up phenomenon predictions in variable vertical load, a) vertical displacement vs. horizontal displacement b) vertical displacement vs. horizontal friction force, (μ = 1.5 μm).

$$\bar{z}_c = y, \quad \bar{z}_l = y + \frac{u}{\bar{\kappa}_w}, \quad \bar{z}_{l1} = y + \frac{\bar{u} - u}{2\bar{\kappa}_w}, \quad \bar{z}_{l2} = y + \frac{\bar{u}}{\bar{\kappa}_w}. \tag{51}$$

Eq. (50) models both the pre-slip and gross slip region, and it is valid for all domains of horizontal displacement. However, it cannot model the butterfly lift-up phenomenon. As an example, the hysteresis friction curves from the MSRI model and the MTRI models for the rough surfaces specified in Table 1 are shown in Fig. 15 (a). The friction hysteresis curves in Fig. 15(a) show that the simpler MSRI model can be employed instead MTRI model with acceptable accuracy in generating hysteresis curves. The MSRI model predictions are also compared in Fig. 15(b) with the classical Mindlin solution (Eriten et al., 2011), which employs a single rough surface (SRS) model without considering the lateral contact effects of asperities. As seen in Fig. 15(b), the proposed MSRI model results in higher friction forces and slippage displacement limits due to considering the effect of lateral contact of asperities in friction coefficient and also including the effect of deformation of asperities dictated by the rod model. It is clear from Fig. 15(b) that the introduction of these effects in the present study significantly influences estimates of the frictional behavior of rough interfaces.

Further investigation on the contact model predictions is performed by verifying asperities that are in stick state satisfy the criterion $\mu \frac{\partial f_n}{\partial f_\tau} \geqslant 1$ (Aleshin and Van Den Abeele, 2013). For the contact that its parameters are specified in Table 1, the values of slippage displacement limits $z \geqslant z_l$ are obtained. Then the product $\mu \frac{\partial f_n}{\partial f_\tau}$ is plotted vs. normalized horizontal displacement, for $u/u_L \leqslant 1$ where, $u_L = \bar{\kappa}_1 \lambda w \, \mathrm{Cos}^2\varphi$ is the maximum displacement of aspirations in the stiction obtained from Eq. (30). As shown in Fig. 16, in the state where the contacting asperities are in stiction (pre-slip), i.e., $u \leqslant u_L$ and $z_L \leqslant z$ the criterion $\mu \frac{\partial f_n}{\partial f_\tau} \geqslant 1$ is satisfied.

4.2. Experimental case study 1: Constant vertical load

The proposed MTRI model predictions are validated experimentally, and its predictions are compared with the results of empirical experiments in vertical constant force condition reported by Eriten

Please cite this article as: H. Jamshidi and H. Ahmadian, A modified rough interface model considering shear and normal elastic deformation couplings, International Journal of Solids and Structures, https://doi.org/10.1016/j.ijsolstr.2020.07.013

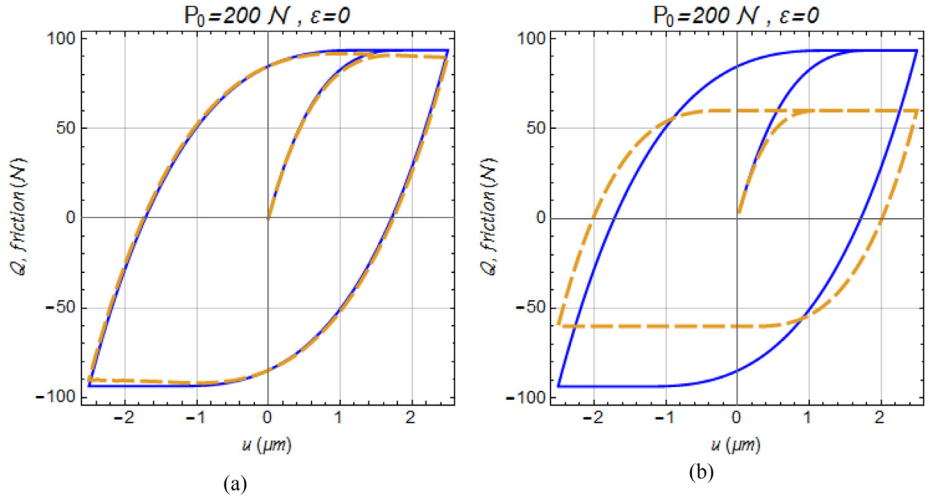

Fig. 15. Comparing hysteresis curves in the slide state, a) MSRI model (solid line) vs. MTRI model (dashed line) predictions, b)MSRI (solid line) vs. Eriten et al. (2011) predictions, CFC model (dashed line).

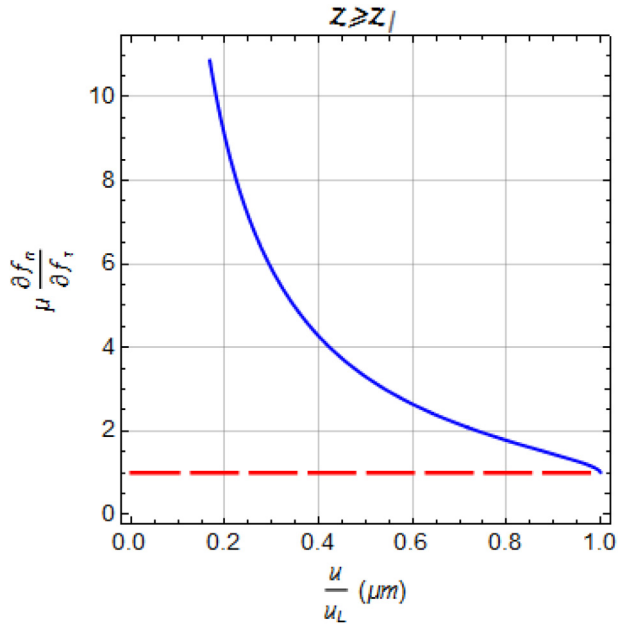

Fig. 16. The plot of $\mu \frac{\partial f_n}{\partial f_\tau}$ vs. $u \leqslant u_L$ in stick state of contacting asperities (solid line).

et al. (2011). The schematic of the experimental setup is shown in Fig. 17.

Mechanical and roughness properties of the contacting surfaces are provided in Table 2. In the measurement of the rough surface profile, if a surface is magnified repeatedly, increasing details of roughness are observed right down to nanoscales. Also, the roughness appears at all magnifications, in which the measured profile consists of roughness on roughness as nanoscale asperities on microscale asperities (Majumdar and Bhushan, 1991). Therefore it requires deciding on what length scale of asperities are to be defined as calculating rough surface parameters of the asperity scale (Barber, 2013; Greenwood and Wu, 2001). The rough surface parameters, used in the Greenwood multi asperity contact model (σ, R, η), are not measured directly but are calculated using measured surface topography (McCool, 1986). The radius of asperity summits (R) and other rough surface parameters (σ, η) are an "intrinsic properties" of a surface. The values of rough surface parameters are related to machining types and processes (Benardos and Vosniakos, 2003).

The asperity radius of R is calculated using a measured profile by a portable contact profilometer (Eriten et al., 2011). Considering the reported roughness data, the parameter, defined in Eq. (46), is set to 3/4.

Information on Table 2 and various amplitudes of horizontal displacement reported by Eriten et al. (2011) are employed to predict the observed hysteresis loop using the proposed model of the present study. Comparisons between observed and experimental behavior in both pre-slip and gross slip state are shown in Figs. 18 and 19. However, it should be reminded that in the MSRI model, the friction coefficient in the proposed formulation is constant. In these figures, the proposed model predictions are compared with the resultant hysteresis curves obtained by BKE model. The BKE model is due to Eriten et al. (2011) and employs classical Mindlin theory and elastic–plastic penetration depth-dependent friction coefficient of Brizmer et al. (2007), to obtain interacting forces at the asperity scale. Through investigation of all penetration depth-dependent friction coefficient models, the BKE model appears to be the most successful in matching the experimental results (Eriten et al., 2011).

Fig. 18, shows that the proposed model generates good predictions in the gross slip mode. The test process, i.e., applied force and deformations is controlled in quasi-static mode (Eriten, 2012), which creates negligible inertia forces of contacting asperities and dynamic behavior of rough interface, leading to conformity between simulation and experimental results. Elastic deflection of asperities is not considered in the proposed model. Therefore, as seen in Fig. 18, the slop of experimental hysteresis curves in the pre-slip region is less than the simulation results. In the test setup, the vertical force of rough interface was provided using bolts, and the assumption of uniformly vertical load distribution is not established through the test. Focusing on the experimental data in Fig. 18 (a), it is evident that in the slip region ($|u| > 2\mu m$), the friction force was slightly increased by the changes in the stiffness of the bolted lap joint. Deviations from the mentioned assumptions are the source of a slight mismatch between analytical and experiment data.

Fig. 19 shows the proposed friction model predictions are also in good agreement with the test results at the pre-slip state under constant vertical force condition.

Please cite this article as: H. Jamshidi and H. Ahmadian, A modified rough interface model considering shear and normal elastic deformation couplings, International Journal of Solids and Structures, https://doi.org/10.1016/j.ijsolstr.2020.07.013

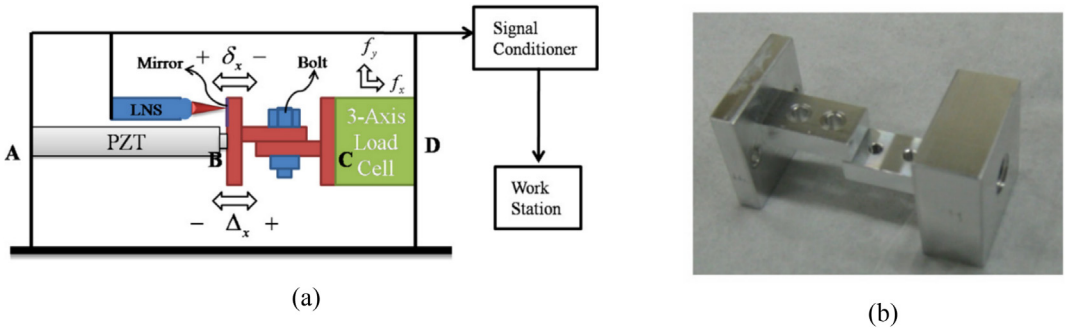

Fig. 17. Constant preload experiments a) experimental setup b) contacting bodies (Eriten et al., 2011).

Table 2
Material properties and topography parameters of the contact surface (Eriten et al., 2011).

Surface roughness parameters		Material and structure properties ($i = u, l$)	
Value	Parameter	Value	Parameter
$2.7\mu m$	σ	$200\,Gpa$	E_i
$44.8\mu m,\ 40.8\mu m$	$R_u,\ R_l$	0.24	υ_i
$30.1\mu m$	$\bar{R}$	$10 \times 17\ mm^2$	A
$2.91 \times 10^{-4}\ \mu m^{-2}$	η	0.3	S/H
4.72	ψ		

An important conclusion inferred from comparisons made in Fig. 18, and Fig. 19, is that the lateral effect of contacting asperities on friction coefficient, which is considered in the present study but neglected by Eriten et al. (2011), plays a vital role in the contact interactions and may not be ignored in multi asperity contact models.

In the proposed elastic model, the Hertzian normal contact force and constant friction coefficient are employed. The plastic behavior of contacted asperities is not considered in the friction and normal force model. However, the resultant curves in Figs. 18 and 19 show that the proposed model also simulates the frictional behavior of rough interfaces in the low plastic region, as $\psi = 4.72$, according to Table 2.

4.3. Experimental case study 2: variable vertical load

In the next case, the contact interface vertical force was not constant where the experimental setup reported by (Rajaei and Ahmadian, 2014) consists of a clamped-frictionally supported steel beam. A suspended mass block at frictionally support provides the desired value for preload, as shown in Fig. 20.

Roughness characteristics of the contact surfaces were obtained from surface roughness measurements and are reported in Table 3. The surface roughness parameters are calculated from the measured surface topography (McCool, 1986). According to Table 3, the values of skewness and kurtosis parameters (R_{sk} and R_{ku}) show that the probability density distribution function of asperity heights is approximately symmetric and is consistent with the Gaussian distribution function (Shi et al., 2019). The roughness characteristics of the contact surfaces are obtained from surface roughness measurements; the calculated radius of asperity summits is $R = 201$ μm. The selection of a length scale of asperities in determining rough surface parameters is arbitrary (Fig. 21).

The test structure was excited near its first resonance frequency using a single harmonic force (Rajaei and Ahmadian, 2014). The single sinusoidal excitation was applied to the beam at different amplitudes to generate acceleration with amplitudes of 1 g, 3 g, and 6 g at the direct point of excitation. At a high level of excitation, micro-vibration impacts initiated in the frictional support leading to variable vertical load in the contact interface.

In Fig. 22, the hysteresis curve at the acceleration response level of 1 g and 3 g is calculated using the proposed model of the present study and compared with the experimental results reported by

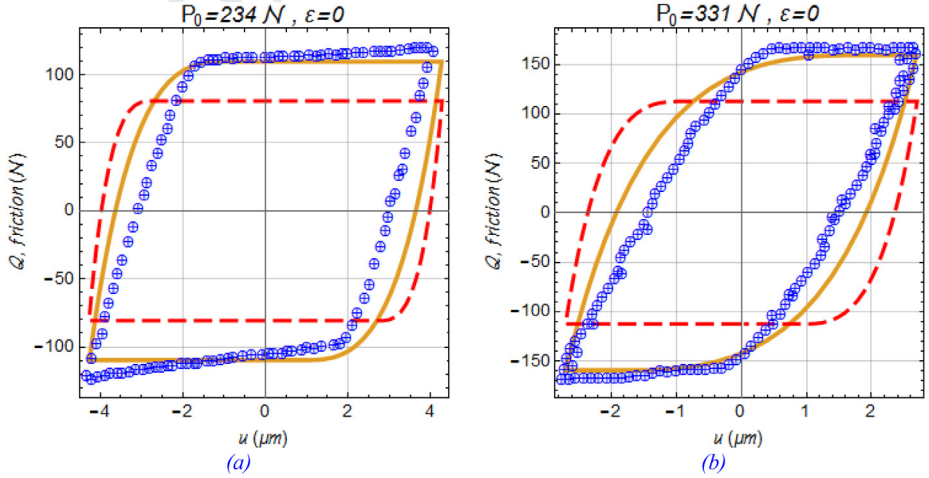

Fig. 18. Comparison of hysteresis behavior under different constant vertical loads in gross slip state (Eriten et al., 2011), Proposed model (solid line), Eriten et al. (2011) proposed BKE model (dashed line), Experimental observations (⊕).

Please cite this article as: H. Jamshidi and H. Ahmadian, A modified rough interface model considering shear and normal elastic deformation couplings, International Journal of Solids and Structures, https://doi.org/10.1016/j.ijsolstr.2020.07.013

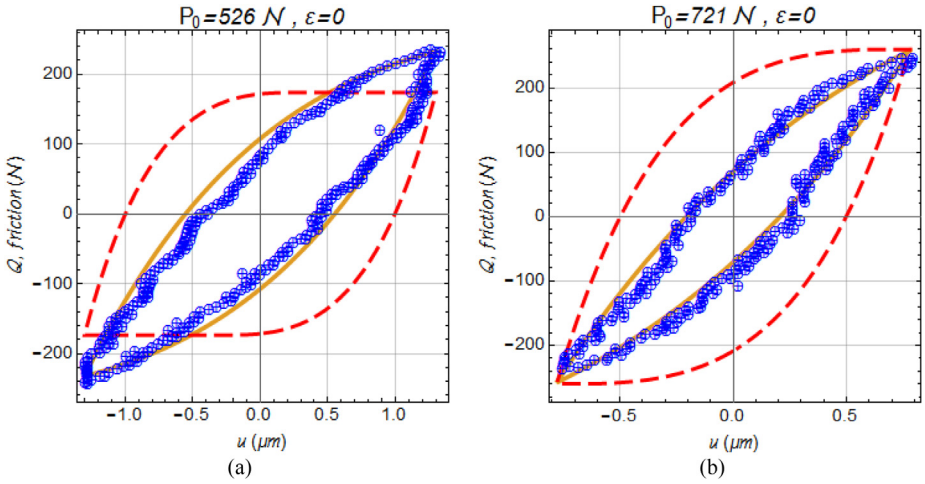

Fig. 19. Comparison of hysteresis behavior under different constant vertical loads in the pre-slip state (Eriten et al., 2011), Proposed model (solid line), Eriten et al. (2011) proposed BKE model (dashed line), Experimental observations (⊕).

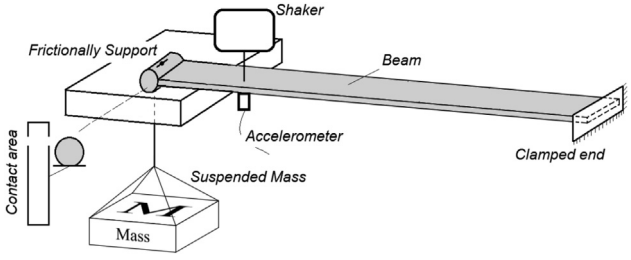

Fig. 20. Schematic of the test setup.

Table 3
Material properties and surface roughness parameters.

Measured surface topography by PS1 and calculated technical data		Material and structure properties ($i = u, l$)	
Value	Parameter	Value	Parameter
$17.5mm,\ 2.5mm$	L_t, L_s	$200\,Gpa$	E_i
$4\mu m,\ 5.9\mu m$	R_a, R_q	0.3	ν_i
3.42 , 0.14	R_{ku}, R_{sk}	0.35	S/H
$52\,/cm,\ 300\mu m$	R_{Pc}, R_{sm}	$100\,mm^2$	A

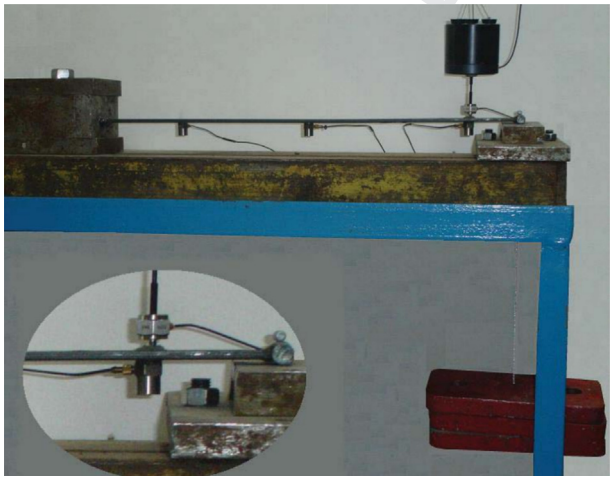

Fig. 21. The test setup.

Rajaei and Ahmadian (2014). At these acceleration levels, the variation of the vertical force produced with 21 kg of mass blocks is negligible. Therefore, the vertical force is considered almost constant. As shown in Fig. 22, the presented model accurately predicts the experimental results. Also, at an acceleration level of 6 g with 3 suspended mass with a total weight of 21 Kg, the proposed model is examined. At this acceleration level, the variation of the vertical force was up to 35% (Rajaei, 2013). As shown in Fig. 23, in this case, the test result and calculated behavior are in good agreement. Also, the comparison of test results with reduced vertical load for another test setup (1 mass block of 7 Kg in 2 g acceleration level) is shown in Fig. 23.

The proposed analytical contact model provides accurate predictions of the observed behavior of the contacting surfaces. The model parameters are directly extracted from contacting surface topography measurements, and there is no need for introducing tuning or updating procedures in the model to match the test results.

5. Conclusion

A two-flat rough interface contact model is developed considering coupling between normal and shear forces and the effects of asperities lateral interactions during shear deformations. The classical Mindlin theory of tangential contact force between elastic spherical asperities is modified by employing rod model instead of Hertz theory, and the effects of contact angle of asperities and deformation friction coefficient are considered in the proposed model. A two-flat rough interface contact model was introduced using the multi-asperity contact theory, and its predictions were validated and verified against experimental observations to ensure its predictability and accuracy. The comparisons show that the proposed contact model predicts the frictional hysteresis behavior accurately in both constant and variable interface normal preload in pre-slip and gross slip modes. Also, it predicts the lift-up deformations phenomenon caused by friction forces. The model predictions signify the effect of lateral contact of asperities in tangential friction hysteresis behavior, which cannot be ignored in the modeling. Based on the proposed MTRI model, a simplified MSRI model is also offered, which considers the side contact effects in the frictional behavior.

Please cite this article as: H. Jamshidi and H. Ahmadian, A modified rough interface model considering shear and normal elastic deformation couplings, International Journal of Solids and Structures, https://doi.org/10.1016/j.ijsolstr.2020.07.013

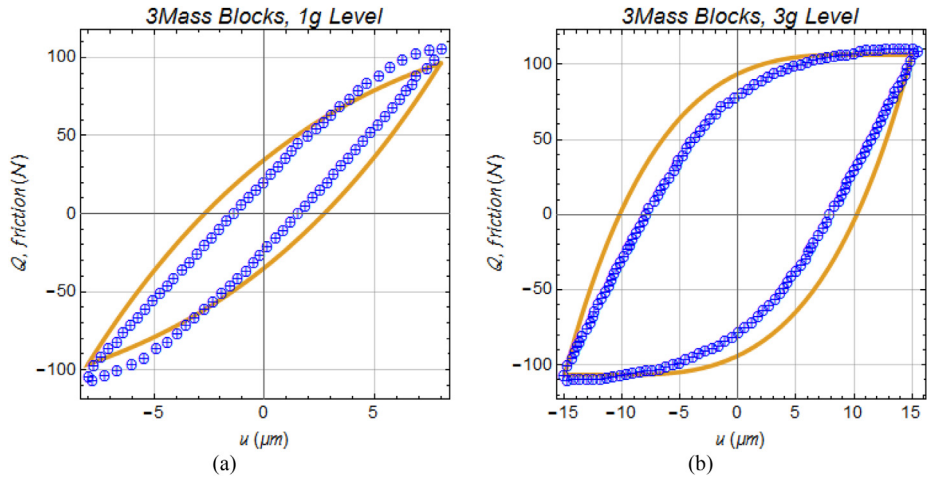

Fig. 22. Predicted hysteresis loop in constant vertical loads condition (solid line), test (⊕).

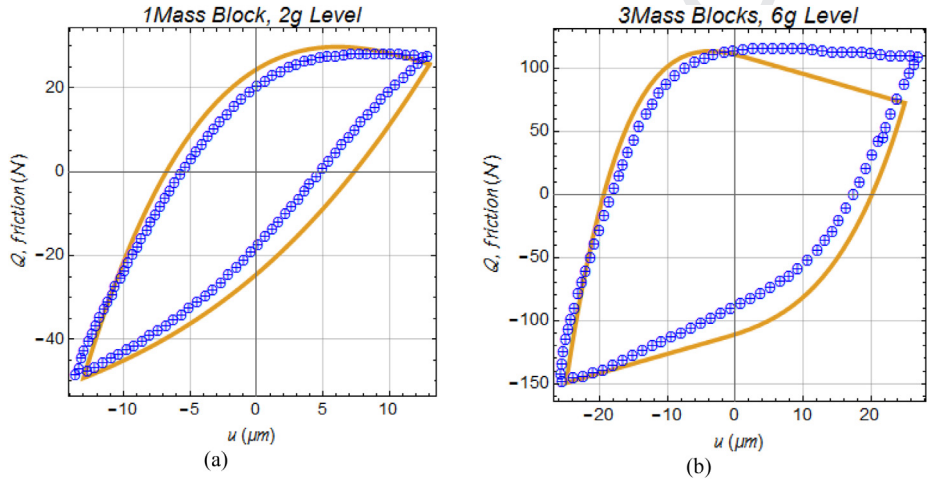

Fig. 23. Predicted hysteresis loop in variable vertical loads condition (solid line), test (⊕).

Declaration of Competing Interest

The authors declare that they have no known competing financial interests or personal relationships that could have appeared to influence the work reported in this paper.

Appendix A:. Modified Mindlin formulation of tangential friction force

Tangential friction force in virgin loading phase in the pre-slip state:

$$f_{\tau,I}^{stick} = s\,\mu(\varphi)\,\kappa_2 K w^{3/2}\mathrm{Cos}^{3/2}\varphi\left(1-\left(1-\frac{1}{\bar{\kappa}_1\lambda}\frac{u}{w\mathrm{Cos}^2\varphi}\right)^{3/2}\right). \tag{A1}$$

Tangential friction force in oscillatory loading phase in the pre-slip saturated state:

$$f_{\tau,II}^{stick} = -s\mu(\varphi)\,\kappa_2 K w^{3/2}\mathrm{Cos}^{3/2}\varphi\left(2\left(1-\frac{1}{2\bar{\kappa}_1\lambda}\frac{\left(s\,u+\bar{u}\right)}{w\mathrm{Cos}^2\varphi}\right)^{3/2}-1\right). \tag{A2}$$

Tangential friction force in oscillatory loading phase in the pre-slip unsaturated state:

$$f_{\tau,III}^{stick} = -s\mu(\varphi)\,\kappa_2 K w^{3/2}\mathrm{Cos}^{3/2}\varphi \left(2\left(1-\frac{1}{2\bar{\kappa}_1\lambda}\frac{\left(s\,u+\bar{u}\right)}{w\mathrm{Cos}^2\varphi}\right)^{3/2}-\left(1-\frac{1}{\bar{\kappa}_1\lambda}\frac{\bar{u}}{w\mathrm{Cos}^2\varphi}\right)^{3/2}-1\right). \tag{A3}$$

Tangential friction force in sliding state:

$$f_{\tau}^{slip} = s\,\mu(\theta)\,\kappa_2 K w^{3/2}\mathrm{Cos}^{3/2}\theta. \tag{A4}$$

where:

$$s = Sgn(\dot{u}) = \begin{cases} -1 & \dot{u} < 0,\ \ unloading \\ 1 & \dot{u} \geqslant 0,\ \ reloading \end{cases}. \tag{A5}$$

- **Horizontal and Vertical Forces:**

Horizontal and vertical forces in the virgin loading phase in the pre-slip state are:

Please cite this article as: H. Jamshidi and H. Ahmadian, A modified rough interface model considering shear and normal elastic deformation couplings, International Journal of Solids and Structures, https://doi.org/10.1016/j.ijsolstr.2020.07.013

$$p_{a,I}^{stick} = f_n \mathrm{Cos}\varphi + f_{\tau,I}^{stick} \mathrm{Sin}\varphi.$$
$$q_{a,I}^{stick} = -f_n \mathrm{Sin}\varphi + f_{\tau,I}^{stick} \mathrm{Cos}\varphi. \quad (A6)$$

Also, in the oscillatory loading phase, saturation state is defined as:

$$p_{a,II}^{stick} = f_n \mathrm{Cos}\varphi + f_{\tau,II}^{stick} \mathrm{Sin}\varphi,$$
$$q_{a,II}^{stick} = -f_n \mathrm{Sin}\varphi + f_{\tau,II}^{stick} \mathrm{Cos}\varphi, \quad (A7)$$

and in the oscillatory loading phase, the unsaturated state is defined as:

$$p_{a,III}^{stick} = f_n \mathrm{Cos}\varphi + f_{\tau,III}^{stick} \mathrm{Sin}\varphi.$$
$$q_{a,III}^{stick} = -f_n \mathrm{Sin}\varphi + f_{\tau,III}^{stick} \mathrm{Cos}\varphi. \quad (A8)$$

Finally, the slip state is defined as:

$$p_a^{slip} = f_n \mathrm{Cos}\theta + f_\tau^{slip} \mathrm{Sin}\theta,$$
$$q_a^{slip} = -f_n \mathrm{Sin}\theta + f_\tau^{slip} \mathrm{Cos}\theta, \quad (A9)$$

where

$$|\mathrm{Sin}\theta| = \left|\mathrm{Sin}\varphi - \frac{u}{2R}\right|. \quad (A10)$$

References

Abdo, J., 2006. Modeling of frictional contact parameters of mechanical systems. Appl. Mech. Eng. 11, 449.
Ahmadian, H., Mohammadali, M., 2016. A distributed mechanical joint contact model with slip/slap coupling effects. Mech. Syst. Sig. Process. 80, 206–223.
Al-Bender, F., De Moerlooze, K., Vanherck, P., 2012. Lift-up Hysteresis Butterflies in Friction. Tribol. Lett. 46, 23–31.
Aleshin, V., Delrue, S., Trifonov, A., Matar, O.B., Van Den Abeele, K., 2018. Two dimensional modeling of elastic wave propagation in solids containing cracks with rough surfaces and friction–Part I: Theoretical background. Ultrasonics 82, 11–18.
Aleshin, V., Van Den Abeele, K., 2013. General solution to the Hertz-Mindlin problem via Preisach formalism. Int. J. Non Linear Mech. 49, 15–30.
Barber, J., 2013. Multiscale surfaces and Amontons' law of friction. Tribol. Lett. 49, 539–543.
Benardos, P., Vosniakos, G.-C., 2003. Predicting surface roughness in machining: a review. Int. J. Mach. Tools Manuf 43, 833–844.
Björklund, S., 1997. A Random Model for Micro-Slip Between Nominally Flat Surfaces. J. Tribol. 119, 726–732.
Boltachev, G.S., Aleshin, V., 2013. Shift and torsion contact problems for arbitrary axisymmetric normal stress distributions. Int. J. Solids Struct. 50, 2894–2900.
Boltachev, G.S., Volkov, N.B., Zubarev, N.M., 2012. Tangential interaction of elastic spherical particles in contact. Int. J. Solids Struct. 49, 2107–2114.
Brizmer, V., Kligerman, Y., Etsion, I., 2007. Elastic–plastic spherical contact under combined normal and tangential loading in full stick. Tribol. Lett. 25, 61–70.
De Moerlooze, K., Al-Bender, F., Van Brussel, H., 2010. A Generalised Asperity-Based Friction Model. Tribol. Lett. 40, 113–130.
Delrue, S., Aleshin, V., Truyaert, K., Matar, O.B., Van Den Abeele, K., 2018. Two dimensional modeling of elastic wave propagation in solids containing cracks with rough surfaces and friction–Part II: Numerical implementation. Ultrasonics 82, 19–30.
Eriten, M., 2012. Multiscale physics-based modeling of friction. University of Illinois at Urbana-Champaign.
Eriten, M., Polycarpou, A.A., Bergman, L.A., 2011. Physics-based modeling for fretting behavior of nominally flat rough surfaces. Int. J. Solids Struct. 48, 1436–1450.
Gao, Z., Fu, W., Wang, W., Lou, L., Wu, J., 2017. Normal Damping Model of Mechanical Joints Interfaces Considering Asperities in Lateral Contact. J. Tribol. 140.
Greenwood, J., Tripp, J., 1970. The contact of two nominally flat rough surfaces. Proc. Inst. Mech. Eng. 185, 625–633.
Greenwood, J., Wu, J., 2001. Surface roughness and contact: an apology. Meccanica 36, 617–630.
Halling, J., 1975. Principles of tribology. Springer.
Hills, D.A., Ramesh, R., Barber, J.R., Moore, M.R., 2018. Methods to solve half-plane partial slip contact problems. Int. J. Solids Struct.
Hintikka, J., Lehtovaara, A., Mäntylä, A., 2016. Normal displacements in non-Coulomb friction conditions during fretting. Tribol. Int. 94, 633–639.
Hutchings, I., Shipway, P., 2017. Friction and Wear of Engineering Materials. In: Hutchings, I., Shipway, P. (Eds.), Tribology. second ed. Butterworth-Heinemann, pp. 37–77.
Jankowski, K., Saha, A., Stefański, A., 2016. Introduction of novel model of friction and analysis of presliding domain of friction with non-local memory effect based upon Maxwell slip model structures. Tribol. Int. 102, 378–391.
Johnson, K.L., 1987. Contact mechanics. Cambridge University Press.
Majumdar, A., Bhushan, B., 1991. Fractal model of elastic-plastic contact between rough surfaces.
McCool, J.I., 1986. Comparison of models for the contact of rough surfaces. Wear 107, 37–60.
Mindlin, R., Mason, W., Osmer, T., Deresiewicz, H., 1951. Effects of an oscillating tangential force on the contact surfaces of elastic spheres. J. Appl. Mech.-Trans. ASME. ASME-AMER Soc. Mech. Eng. 10017, 331. 345 E 47TH ST NEW YORK, NY.
Misra, A., 2002. Effect of asperity damage on shear behavior of single fracture. Eng. Fract. Mech. 69, 1997–2014.
Misra, A., Huang, S., 2011. Effect of loading induced anisotropy on the shear behavior of rough interfaces. Tribol. Int. 44, 627–634.
Misra, A., Huang, S., 2012. Micromechanical stress–displacement model for rough interfaces: Effect of asperity contact orientation on closure and shear behavior. Int. J. Solids Struct. 49, 111–120.
Panagouli, O.K., Mastrodimou, K., 2017. Dependence of friction coefficient on the resolution of asperities in metallic rough surfaces under cyclic loading. Int. J. Solids Struct. 108, 85–97.
Rajaei, M., 2013. Identification of Iwan distribution density function in a mechanical joint interface. University of Science and Technology, Tehran. Iran, Department of Mechanical Engineering.
Rajaei, M., Ahmadian, H., 2014. Development of generalized Iwan model to simulate frictional contacts with variable normal loads. Appl. Math. Model. 38, 4006–4018.
Sepehri, A., Farhang, K., 2008. On elastic interaction of nominally flat rough surfaces. J. Tribol. 130, 011014.
Sepehri, A., Farhang, K., 2011a. Closed-form equations for contact force and moment in elastic contact of rough surfaces. Model. Simulat. Eng. 2011, 25.
Sepehri, A., Farhang, K., 2011b. A finite element-based elastic-plastic model for the contact of rough surfaces. Model. Simulat. Eng. 2011, 16.
Shi, R., Wang, B., Yan, Z., Wang, Z., Dong, L., 2019. Effect of Surface Topography Parameters on Friction and Wear of Random Rough Surface. Materials 12, 2762.
Shi, X., Zou, Y., Fang, H., 2016. Numerical Investigation of the Three-Dimensional Elastic-Plastic Sloped Contact Between Two Hemispheric Asperities. J. Appl. Mech. 83.
Truster, T.J., Eriten, M., Polycarpou, A.A., Bergman, L.A., Masud, A., 2013. Stabilized interface methods for mechanical joints: Physics-based models and variationally consistent embedding. Int. J. Solids Struct. 50, 2132–2150.

Please cite this article as: H. Jamshidi and H. Ahmadian, A modified rough interface model considering shear and normal elastic deformation couplings, International Journal of Solids and Structures, https://doi.org/10.1016/j.ijsolstr.2020.07.013